Neuronal Silencing and Protection in a Mouse Model of Demyelination

Aniruddha Das,[1, †] Julie Borovicka,[1, †] Hale Tobin,[1] Shruti Bhatia,[1] Jacob Icardi,[1] Ghazaal Tahmasebi,[1] Priyanka Agochiya,[1] Shriya Singh,[1] Jordon Manworren,[1] Philopater Isak,[1] Bruce Trapp[1] and Hod Dana[1,2,*]

[†]These authors contributed equally to this work.

1 Department of Neurosciences, Lerner Research Institute, Cleveland Clinic Foundation, Cleveland, OH 44195, USA

2 Department of Molecular Medicine, Cleveland Clinic Lerner College of Medicine of Case Western Reserve University School of Medicine, Cleveland, OH 44195, USA

Correspondence to: Hod Dana

Department of Neurosciences, Lerner Research Institute

Cleveland Clinic Foundation, Cleveland, OH 44195, USA

e-mail danah@ccf.org

Keywords: Cuprizone model; calcium imaging; two-photon microscopy; third-harmonic generation microscopy; Clemastine Fumarate.

Abstract

Damage to the myelin sheath that protects axons in the central nervous system is a hallmark pathology of demyelinating diseases like multiple sclerosis. Cuprizone-induced demyelination in mice is a common model for studying demyelination and remyelination. However, the relationship between myelin damage and recovery and neuronal function remains poorly understood. By monitoring hippocampal myelination and neuronal activity in the same mice, we assessed longitudinal changes following cuprizone consumption and remyelination treatment. Upon cuprizone consumption, a rapid decline in neuronal activity preceded slower demyelination. Female mice showed a more intense early decrease in brain activity and a stronger correlation with levels of myelin loss. Remyelination treatment led to increased myelination levels and recovery of neuronal activity compared to vehicle treatment. Changes in single-neuron firing rates during treatment were proportional to the pre-cuprizone firing rate in

the same cells, highlighting a potential linkage between the status of myelin recovery and cellular activity.

Introduction

Myelin is a multi-layered sheath that is produced by oligodendrocytes, insulates axons, and enables the rapid transmission of action potentials[1]. In demyelinating diseases like multiple sclerosis (MS), myelin degeneration leads to severe symptoms, including speech, motor, and visual deficits, along with long-term cognitive decline[2, 3]. Cognitive and memory loss in MS patients are linked to hippocampal demyelination and atrophy[2, 4]. While MS is recognized as a disease with a major autoimmune inflammatory component, basic studies, human tissue biopsies, and patient autopsies suggest that primary oligodendrocyte dystrophy also contributes to its development[5, 6].

Rigorous study of demyelination-related pathologies requires the use of an appropriate animal model, especially since patient tissue is usually limited to the late stages of the disease[7]. Such an established model is the mouse cuprizone model[8]. Cuprizone is a copper chelator, which induces selective death of mature oligodendrocytes in the brain, leading to extensive demyelination, including in the hippocampus. Additionally, this model allows studying remyelination processes that occur spontaneously after cessation of cuprizone consumption[8, 9]. Previous studies showed gradual brain-wide demyelination that typically begins 2-3 weeks after cuprizone initiation and continues as long as it is consumed[10].

Previous reports have found that cuprizone-induced hippocampal demyelination alters CA1 neuronal function and long-term potentiation in tissue slices[4, 11]. We found reduction of hippocampal neuronal firing *in vivo* during cuprizone consumption, with partial recovery upon returning to regular diet[12]. Partial remyelination was shown to be sufficient to restore cortical function following therapeutically-enhanced oligodendrogenesis[13]. However, the relationship between de/remyelination and neuronal functionality is still poorly understood.

In this study, we longitudinally recorded two-photon laser scanning microscopy (TPLSM) fluorescence from CA1 neurons of transgenic mice expressing the jRGECO1a calcium sensor to monitor their firing rates (FRs)[14, 15]. Concurrently, we recorded third-harmonic generation (THG) signals from the same mice. THG produces label-free signals from areas rich in lipids, like myelin, which enables monitoring of their myelination status[16, 17]. Upon cuprizone

consumption, we found a rapid reduction in neuronal FRs alongside gradual demyelination. Male and female mice showed different neuronal activity reduction patterns, and a correlation between neuronal activity reduction and myelin loss was found in females only. Following cuprizone cessation, mice were treated with Clemastine, a drug currently in clinical trials for MS patients, to enhance remyelination[18, 19]. This treatment also restored neuronal FR levels to their pre-cuprizone levels.

Results

Longitudinal monitoring of neuronal activity and myelin status

TPLSM and THG were used to record firing of CA1 pyramidal neurons and to monitor their hippocampal myelination status, respectively (Fig. 1A-B). All mice were randomly assigned to two groups. The cuprizone group was fed with 0.3% cuprizone diet for 55 days, followed by 45 days of daily treatment with Clemastine or vehicle (Fig. 1C). The control group was fed with regular diet for the entire study period and received no treatment. Identical THG and TPLSM recording sessions were conducted at selected timepoints to monitor longitudinal changes in neuronal activity, myelin condition, and body weight (Fig. 1D-F, Supplementary. Fig. 2).

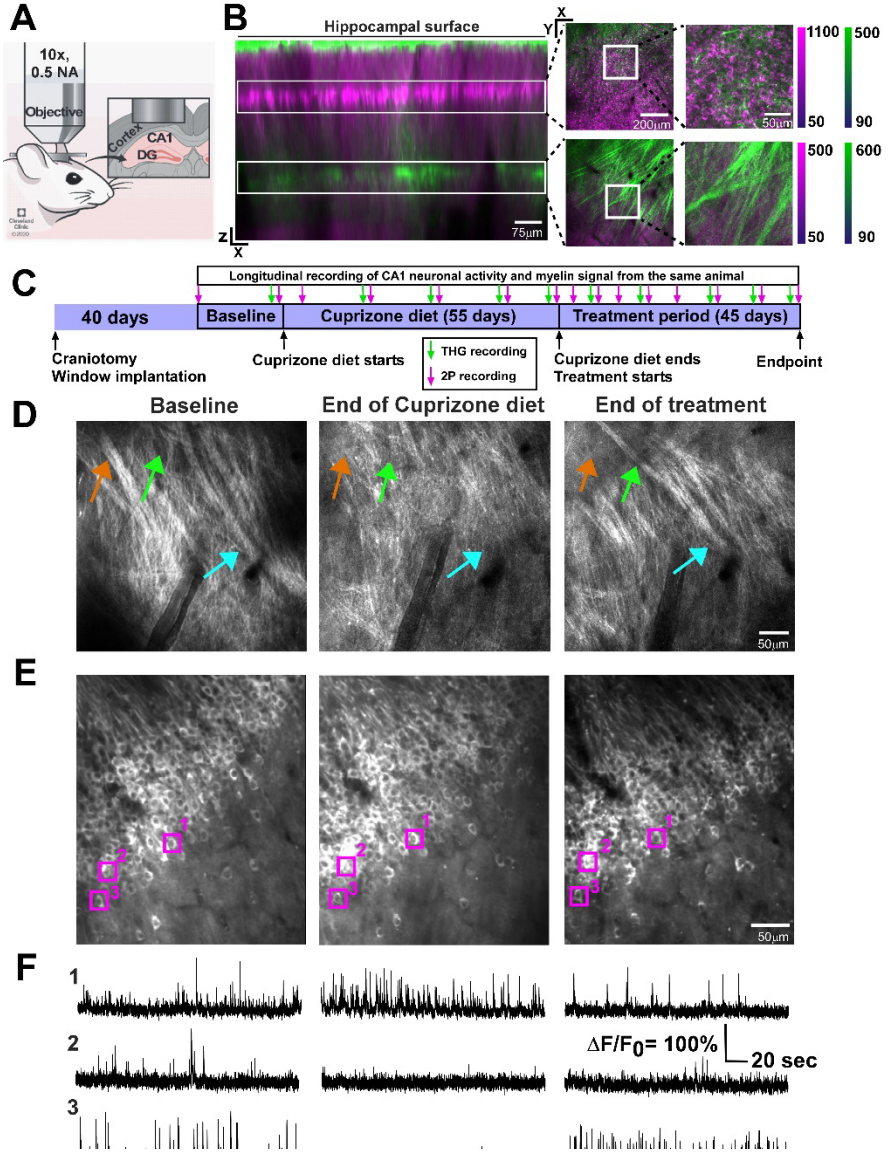

Figure 1: Longitudinal monitoring of hippocampal CA1 activity and myelination levels in a mouse model of de/remyelination. (A) Illustration of hippocampal window implantation to allow long-term access to the hippocampus of a Thy1-jRGECO1a mouse. **(B)** *In vivo*

side view of a Thy1-jRGECO1a hippocampus shows CA1 neurons, axons, and dendrites expressing the red calcium sensor jRGECO1a (acquired by TPLSM and shown in magenta) and hippocampal myelin (acquired by THG and shown in green). Insets: horizontal views of the CA1 and myelinated fiber layers. **(C)** Timeline for neuronal activity and myelin recording sessions (indicated by magenta and green arrows, respectively). **(D)** Example THG images from the same FOV show the disappearance (at Cuprizone Day 55, orange and cyan arrows), reappearance (cyan arrows), and newly-appearing myelin fibers (green arrows) during the cuprizone consumption and recovery periods. **(E)** Example TPLSM images from the same FOV of CA1 neurons expressing jRGECO1a. The same cells are highlighted by the numbered magenta squares in the different images. **(F)** Raw fluorescence traces of the cells shown in E. Firing of action potentials causes an increase in the fluorescence signal.

Sex-specific patterns of CA1 activity loss during cuprizone consumption

Following cuprizone consumption, the myelin signal gradually decreased from its baseline levels and showed a significant decrease after 32 days of cuprizone diet, without significant sex differences (Fig. 2A). The neuronal FR significantly decreased from baseline activity levels after 4 days of cuprizone diet and remained significantly lower than baseline levels for the entire duration of cuprizone diet (55 days). Female mice showed significantly lower CA1 FRs than males on cuprizone day 4. Then, CA1 FRs slightly recovered and were comparable in both sexes during days 18-32. Finally, a second decrease was detected in days 46-55, which was more severe in male mice and led to significantly lower FRs in males on CD55 compared to females (Fig. 2B).

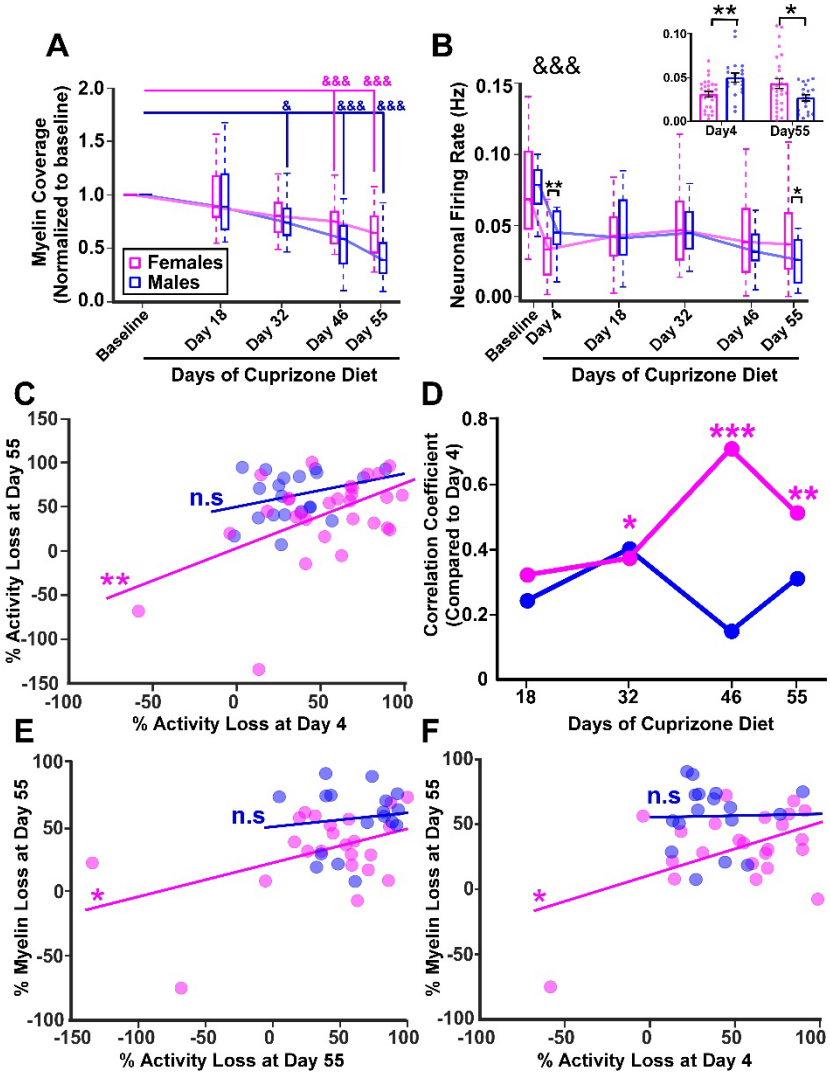

Figure 2: Loss of brain activity and correlations between cuprizone-induced functional and morphological pathologies are sex-specific. (A) Myelin coverage gradually decreased following cuprizone consumption without sex differences (*n*=43, 17 males and 26 females; values are normalized to the same-mouse baseline levels; linear mixed-effect model with Dunnett's *post hoc* comparisons, &,

P<0.05, &&&, *P*<0.001 for time effect). Boxplots show medians and 25-75 quartiles, and the whisker length is the shorter of 1.5 times the inter-quartiles range or the extreme data point. **(B)** CA1 FRs showed significant decreases from baseline levels in both male and female mice. Females showed a significantly larger decrease than males on CD4 and males showed a significantly larger decrease than females on CD55 (*n*=48 mice, 19 males and 29 females; females: 250-3525 neurons/mouse, median=1083 neurons; males: 158-3207 neurons/mouse, median 1178 neurons; linear mixed-effect model with Tukey's HSD. Inset shows individual mouse data points and the group average and SE on CDs 4 and 55 (*P*=0.0036 and 0.018 respectively). *, *P*<0.05, **, *P*<0.01 for sex differences. **(C)** Same-mouse reduction of CA1 FR (%) from baseline to CD4 vs. from baseline to CD55 were correlated among females, but not males (*r*=0.51 and *P*=0.0047 for females vs. *r*=0.31 and *P*=0.20 for males; Pearson's correlation was used for C-F. The correlation coefficient *(r)* and significance *(P)* are reported). **(D)** Summary of the Pearson's *r* value for FR reduction (%) from baseline to CD4 vs. from baseline to all other cuprizone recording days. *, *P*<0.05; **, *P*<0.01; ***, *P*<0.001. **(E)** Same-mouse reduced CA1 FR (%) and the loss of myelin coverage (%) from baseline to CD55 were correlated for females (*r* =0.45, *P*=0.033), but not for males (*r* =0.12, *P*=0.65). **(F)** Same-mouse reduced CA1 FR (%) from baseline to CD4 and the loss of myelin coverage (%) from baseline to CD55 were also correlated for females (*r* =0.49, *P*=0.018), but not for males (*r* =0.02, *P*=0.93). Additional details may be found in the Supplementary Statistical Data.

Correlated brain activity and demyelination levels during cuprizone consumption

We assessed whether the rapid decrease in FR from baseline to CD4 was correlated with FR levels in the same mice on other recording days. We found significant positive correlations for female mice on recording days 32, 46, and 55, but no significant correlations for males (Fig. 2C-D). Moreover, there was a significant correlation between the percent loss of CA1 activity on CD55 and the percent of myelin signal loss on the same day (Fig. 2E) in females, but not in males. Finally, a significant correlation was also found between loss of CA1 activity on CD4 and the loss of myelin on CD55 in the same females, which was also not observed in the same males (Fig. 2F).

Clemastine remyelination treatment restores CA1 firing rates

Following 55 days of cuprizone diet, mice in the cuprizone group were switched to regular diet and were randomly assigned into one of two groups. The Clemastine group received daily oral gavage treatment of Clemastine for 45 days, and the vehicle group was similarly treated with vehicle solution only. In agreement with previous studies, Clemastine-treated mice showed increased remyelination compared to vehicle-treated mice, as measured by increased myelin coverage as well as the signal amplitude and thickness of myelinated fiber tracts (Fig. 3A-C). For the first 6 days after cuprizone cessation, there was a small increase in myelination coverage in both groups. Then, the vehicle group showed a significant monotonic downward trend and the Clemastine group showed a significant monotonic upward trend for the remaining treatment days

(Fig. 3D). A similar pattern was evident with CA1 FR, when a short-term increase was measured in both groups over the first 6 treatment days, followed by a significant monotonic downward trend in the vehicle group and a gradual increase in the Clemastine group. These different patterns led to a significant effect of Clemastine treatment on CA1 FR levels between the Clemastine and vehicle groups on TD45 (Fig. 3E). No significant changes were found in FR or myelination in the control group (Supplementary Fig. 3). Comparison with proteolipid-protein-stained samples, which were collected at the study endpoint, showed non-significantly higher myelin coverage in the control group compared to the Clemastine group, with the lowest coverage being in the vehicle group (Supplementary Fig. 4).

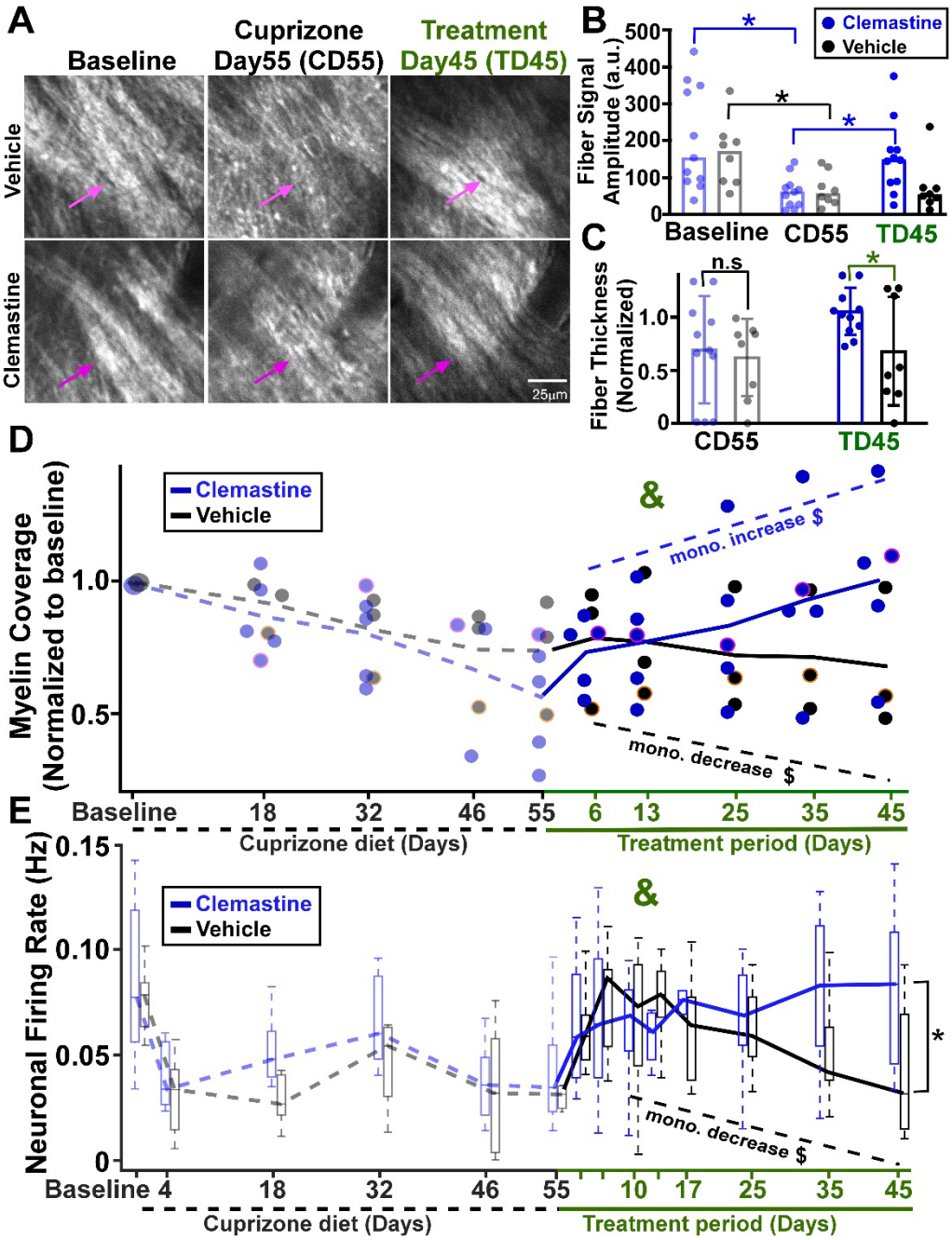

Figure 3: Clemastine treatment restores brain activity levels. (A) THG images of the same fiber tracts on baseline, CD55, and TD 45. Arrows indicate the same fibers in the different images (images are contrast-enhanced). **(B-C)** Cross-sections of individual fibers were fit with a Gaussian function to estimate their amplitude over their surrounding (**B**) and thickness (**C**; Clemastine group: n=11 fibers from 5 mice; vehicle group: n_1=8 fibers from 3 mice; values are normalized to the same-fiber baseline thickness). Until CD55, both groups showed significant decreases in fiber thickness and amplitude. Clemastine treatment, but not vehicle, significantly increased both fiber thickness and amplitude (Fiber amplitude: two-way ANOVA with HSD; Fiber thickness: unpaired Student's t-

test). (**D**) Following treatment, the mean myelin coverage monotonously increased for Clemastine-treated mice and decreased for vehicle-treated mice, leading to a significant difference (*n*=8 mice, 5 Clemastine and 3 vehicle; *P*=0.028 in both groups, Mann-Kendall test, indicated by $. Two-way ANOVA analysis from TD6 to TD45 showed a significant time-group interaction, *P*=0.038, indicated by &). Each dot shows data from one mouse; pale and dotted lines connect the means during the cuprizone diet period and dark and solid lines during the treatment period. Dots with magenta/orange borders show the example data in A. **(E)** Clemastine treatment enhanced the mean CA1 FR compared to vehicle (*n*=15 mice, 8 Clemastine and 7 vehicle; Clemastine: 321-3207 neurons/mouse, median=985 neurons; vehicle: 250-3021 neurons/mouse, median=915 neurons). Same-mouse CA1 FR was longitudinally recorded during the cuprizone diet and treatment periods (pale/dotted and dark/solid lines/boxplots, respectively). During the first 6 days of the treatment period, the FRs in both groups increased. From TD10 until the study endpoint, the vehicle group mean FR monotonously decreased (*P*=0.024, Mann-Kendall test). The Clemastine group FR recovered back to its baseline levels, leading to a significant difference between the groups on TD45 (*P*=0.049; linear mixed-effect model with HSD, *P*=0.033 for time-group interactions). Boxplots show medians and 25-75 quartiles, and the whisker length is the shorter of 1.5 times the inter-quartiles range or the extreme data point. Additional details may be found in the Supplementary Statistical Data.

Cellular-level responses to treatment

In a subset of the cuprizone mice, the same neurons were monitored throughout the entire study period. Same-cell activity was compared between baseline, CD55, TD10, and TD45 (Fig. 4A). We checked whether cellular properties, such as the neuronal baseline FR, was correlated with the early and late recovery patterns that were identified (Fig. 3E). Between CD55 and TD10, the change in FR of neurons in the Clemastine group showed no dependency on baseline FR. However, for vehicle neurons, a positive correlation with baseline FR was found, indicating that cells with high baseline FR showed larger increases on average between CD55 and TD10 (Supplementary Fig. 5). Interestingly, between TD10 and TD45, the effect of treatment has the opposite correlation with same-cell baseline FR for each group. For Clemastine neurons, a higher baseline FR was correlated with a higher mean FR increase, while for vehicle neurons, it was correlated with a bigger decrease (Fig. 4E). Finally, the variability of the mean increase/decrease in FR also increased with the baseline FR (Fig. 4F).

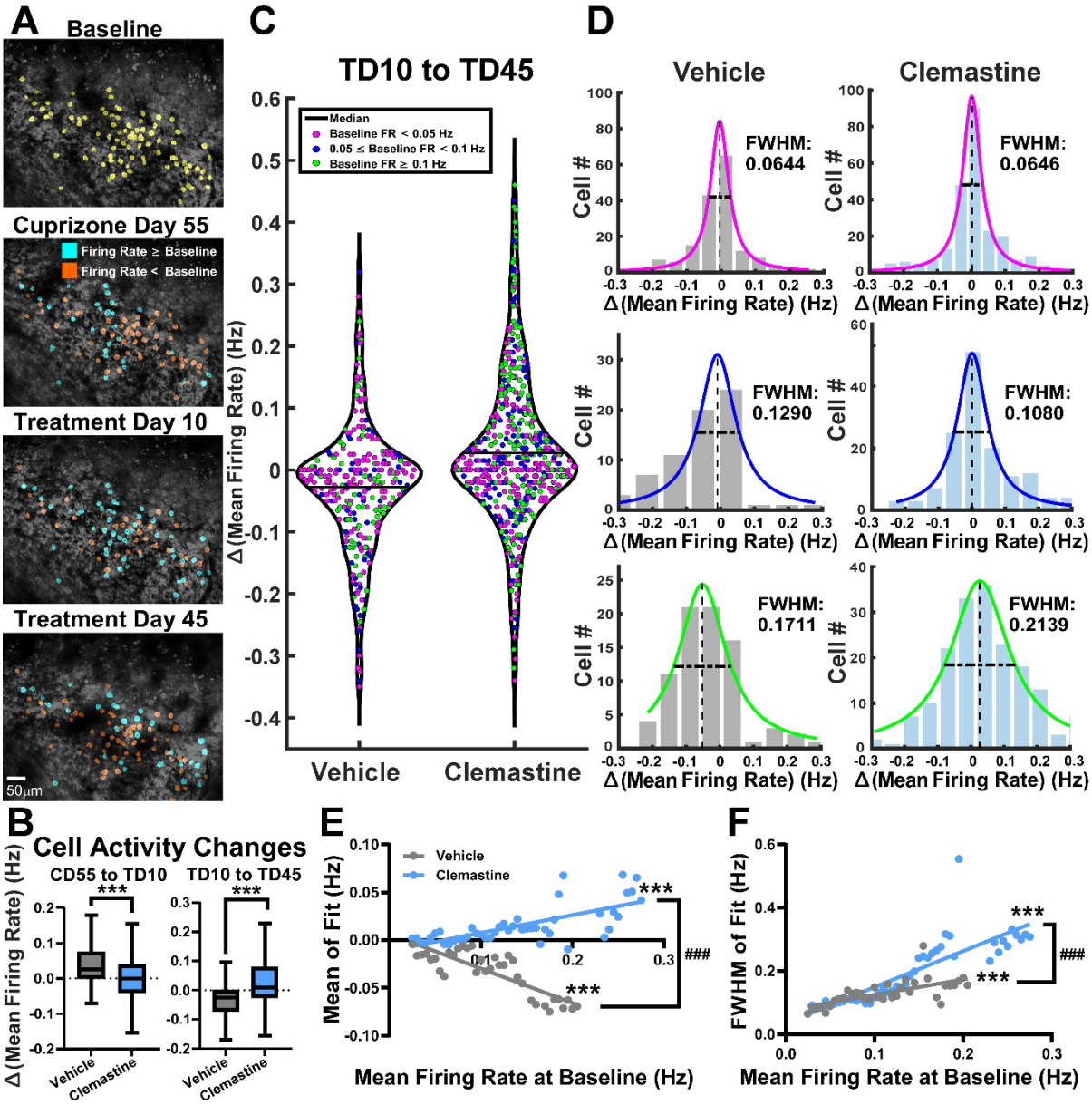

Figure 4: Single-cell correlates of recovery during Clemastine treatment. (A) Example of tracking the same cells over baseline, CD55, TD10, and TD45 (*n*=87 cells, shown in yellow in the baseline image). Cyan- and orange-labeled cells exhibited higher and lower FR than their baseline levels, respectively. **(B)** Distributions of the changes in same-cell FR from CD55 to TD10 (left) and from TD10 to TD45 (right) for the vehicle and Clemastine groups (*n*=6, 3 mice per group, with 165 and 336 same-cells in the vehicle and Clemastine groups, respectively). The vehicle group showed a significantly higher increase between CD55 to TD10 than the Clemastine group (*P*<0.0001, unpaired Student's t-test), followed by a decrease from TD10 to TD45. The Clemastine group showed an increase between TD10 to TD45, which was significantly higher than the vehicle group (*P*<0.0001, unpaired Student's t-test). **(C)** Violin plot of the changes in same-cell FRs between TD10 to TD45, where the color of each dot indicates whether the baseline FR of the cell was high, medium, or low (*n*=306 and 553 cells from vehicle and Clemastine groups, respectively). **(D)** Histograms of low-, medium-, and high-baseline FR cells from C were fitted with Lorentzian functions. The data show that neurons with high baseline activity tended to have larger FWHM values. Moreover, their mean change was positive for Clemastine and negative for vehicle. **(E)** The same cells from C were grouped

into partially-overlapping bins based upon their baseline FRs and their histograms were fitted with Lorentzian functions as in D. The means of the Lorentzians were positively correlated with the same-cell baseline FR in the Clemastine group and were negatively correlated in the vehicle group (Clemastine, r=0.7024, vehicle, r= -0.8451; P<0.001 for both groups, Pearson's correlation). **(F)** Both groups showed an increase in variability (FWHM) with the increase of same-cell baseline FR (Clemastine, r=0.8436, vehicle, r=0.6602; P<0.001 for both groups). ***, P<0.001 significance of Pearson correlation; ###, P<0.001, significance of ANCOVA test for checking significant difference in the fit lines' slopes.

Discussion

This work presents a novel *in vivo* approach to longitudinally measure both brain activity and myelination of axons from the same animal throughout toxin-induced demyelination and remyelination treatment. It was previously shown that neuronal activation promotes myelination via oligodendrogenesis in the mouse brain[20]. This study identifies that for the cuprizone model of demyelination, loss of brain activity precedes the physical loss of myelin. Moreover, the functional decrease in CA1 FR only 4 days after cuprizone administration can predict the level of myelin loss in the same mouse after 55 days of cuprizone consumption (Fig. 2). This relationship between myelination and cellular activity is further expanded by the finding that Clemastine treatment enhances both remyelination and CA1 FR. These findings, which are based on data from the same mouse, suggest a potential bi-directional interaction between cellular activity and myelination level. This study design is limited in its ability to link single-cell activity and myelination levels of the same cell; therefore, more detailed conclusions will require future studies.

We found sex-specific differences in the measured brain activity patterns. Female mice showed a more severe decline in CA1 activity within 4 days of cuprizone consumption, while males exhibited a more severe decline after 55 days of cuprizone. For female mice, but not for males, the correlations of the FR loss with CD4 increased over time (Fig. 2D-E). This suggests that cuprizone-induced neuronal silencing in females, especially the rapid component that is apparent after 4 days, is not random and is largely maintained throughout the 55 days of cuprizone consumption. Notably, females are predisposed to MS relapses more than males[21], which makes demyelination-related sex differences a question with potential translational directions. These findings suggest that neuronal activity recording reveals some of the underlying sex differences that are not apparent by recording myelin condition alone.

Remyelination therapy may alleviate the condition of MS patients, especially during progressive stages of the disease[22]. Clemastine enhances myelin repair (Fig. 3B-D), presumably

by enhancing the maturation of myelinating oligodendrocytes[23]. Our findings demonstrate that it also significantly restored neuronal FR compared to vehicle-treated mice to levels close to baseline FRs (Fig. 3E). Therefore, Clemastine's neuroprotective effects extend beyond regenerating myelin only; it also protected the neuronal activity that may have further declined due to cuprizone consumption. Moreover, Clemastine treatment increased the FR of individual neurons in a proportional manner to their baseline FR. This effect was opposite to neurons in the vehicle group (Fig. 4E). This suggests that the neuroprotective effects of Clemastine interact with intrinsic cellular properties, such as the baseline FR, and may have additional cell-specific characteristics that are yet to be established. We note that the increased complexity of completing long-term monitoring of baseline recording, 55 days of cuprizone diet and 45 days of treatment, prevented us from recording a sufficient number of mice to identify potential sex differences in recovery. We also note that only one Clemastine dose was studied, so therefore we could not identify dose-dependent effects of Clemastine on CA1 FRs. Finally, the effect of Clemastine on neuronal activity may also have negative consequences, and may be related to complications in clinical trials with Clemastine that were recently reported[24].

Materials and methods

All surgical and experimental procedures were conducted in compliance with protocols approved by the Institutional Animal Care and Use Committee and Institutional Biosafety Committee of the Lerner Research Institute. The ARRIVE guidelines were used to report the below findings[25].

Surgical procedures

Thy1-jRGECO1a mice (10-12 weeks old) were implanted with hippocampal windows above their left hippocampus following published protocols[15, 26, 27]. Briefly, mice were anesthetized using isoflurane (3% for induction, 1.5% during surgery), the scalp skin was removed, and a circular craniotomy was drilled through the skull (3.2mm diameter, -2/-2 mm AP/ML from Bregma, OMNIDRILL35, WPI). The cortex and corpus callosum tissue above the hippocampus were aspirated, while leaving the hippocampus intact. A glass coverslip (3mm diameter #1 glass, Warner Instruments) attached to a metal cannula (2.65/3.2mm internal/outer diameters, 1.8mm length, New England Small Tube Company, 304L stainless steel) was placed above the hippocampus. The cannula and a headbar were secured to the skull using dental cement (Contemporary Ortho-Jet) and a cyanoacrylate glue.

Longitudinal recordings

Mice were intramuscularly injected with Chloroprothixene Hydrochloride (30µl of 0.33mg/ml, Spectrum Chemical) and were kept on a 37°C heating pad under light anesthesia (0.5-0.75% isoflurane)[12]. TPLSM was used to record spontaneous activity of CA1 pyramidal neurons expressing jRGECO1a using 1100 nm excitation light (100-200mW, Insight X3, Spectra-Physics), a 10x 0.5 NA objective (TL10X-2P, Thorlabs), and a Bergamo II microscope (Thorlabs) equipped with resonant/galvo scanners and a GaAsP PMT detector (512x512 pixels, 600x600μm^2, 30frames/sec, 607/70nm emission filter, Semrock). Three to five fields of view (FOVs) were typically collected for 200 seconds each. One to two baseline recordings were conducted before the initiation of cuprizone diet, as well as on cuprizone days (CDs) 4, 18, 32, 46, and 55, and subsequently on treatment days (TDs) 3, 6, 10, 13, 17, 25, 35, and 45. Recording days were selected to capture the expected early changes at the beginning of cuprizone and treatment periods, and then to monitor the longitudinal changes. All recording sessions were performed identically. For n=6 mice, the same neurons within each FOVs were re-located every session. For all other mice, the same area within CA1 was recorded, but not the same cell.

THG recordings were conducted using the same microscope using low-repetition-rate laser at 1260 nm excitation wavelength (15-60 mW, Carbide 40W laser and Orpheus-F OPA, Light Conversion) using galvo-galvo scanners and a GaAsP PMT detector (1024x1024 pixels, both 200x200 and 400x400 μm^2 FOVs were acquired, ~1-2 frames/sec, 434/32nm detection filter, Semrock). To minimize the risk of heat-induced damage, recordings were conducted once during baseline, and on CDs 18, 32, 46, and 55, and then on TDs 6, 13, 25, 35, and 45.

Mouse model of demyelination and remyelination

Mice were kept in standard housing (12-hour light/dark cycle, access to food and water *ad libitum*) and were given 4-7 weeks for post-craniotomy recovery before recordings were initiated. After initiating recording in a portion of the mice, we identified that a minimum period of 40 days is needed to achieve full recovery, as reflected in stable CA1 activity. Hence, only mice that had at least one baseline recording after 40 or more days post-craniotomy were included in the study and the rest were excluded (n=25, Supplementary Fig. 1). Following the baseline recordings, mice were randomly assigned into two groups. The cuprizone group was fed

with 0.3% cuprizone diet (TD. 140805, Envigo), while the control group continued with regular diet. The cuprizone pellets were stored at 4°C and replaced three times/week. Following 55 days of cuprizone diet, the mice were switched back to regular diet for an additional 45 days until the study's endpoint. Mice were weighed on each recording day.

Following the cessation of cuprizone diet, mice in the cuprizone group were randomly divided into two groups. For one group, mice were treated daily in a random order with Clemastine (Sigma-Aldrich; 10 mg/kg of body weight. Mice were oral gavaged with a solution of 1.33 mg/ml Clemastine Fumarate in 90% H_2O, 5% Tween-20, and 5% DMSO). The second group received identical treatment using the vehicle solution only. Mice that were removed from the study during the cuprizone or treatment phases due to health or window quality concerns were excluded from the analysis (n=36, Supplementary table 1). No blinding was used.

Data analysis

Analyses were based upon custom MATLAB scripts (MathWorks), similar to our previous work[12]. Raw fluorescence movies were registered in order to correct for small movements[28]. Somatic regions of interest (ROIs) were segmented using CellPose[29]. Pixels of each ROI were averaged to calculate the time-dependent fluorescence signal (F). Baseline fluorescence (F_0) was estimated as the median of F. Action potential (AP) number was estimated using the SpikeML algorithm using jRGECO1a parameters[14, 30]. Myelin coverage was quantified by applying two thresholds on the raw images using Otsu's method and calculating the ratio of the brightest pixels vs. all pixels. Myelin fiber properties were measured by fitting a Gaussian function to cross-sections of the same visually-identified fibers across different images. Thickness was defined as the fit's full width at half maximum (FWHM). The amplitude was defined as the maximum of the fit minus its minimum. All recordings were inspected for quality issues, like movement artifacts and relocation of the same myelinated fibers. In case issues were found, the specific session was excluded (TPLSM recordings: n_1= 9 sessions from n_2= 9 mice; THG recordings: n_1= 22 sessions from n_2= 18 mice, Supplementary Table 2). Data from the same cells were compared across four days: baseline, CD55, TD10, and TD45. The segmented FOVs were compared using a probabilistic model of cell centroid distances to identify the same cells[31]. The same-cell FRs were calculated, and outliers were excluded using the ROUT method (Q = 0.01). Separately, cells which were identified just in the [baseline, TD10, and TD45] or [baseline, CD55 and TD10] datasets, were also excluded of outliers (ROUT, Q = 0.01) and binned into

partially-overlapping bins of +/- 0.025 Hz baseline FRs. We calculated histograms of change in average FR from TD10 to TD45 or CD55 to TD10 for each bin, which were fitted with scaled Lorentzian functions: $Y = a/(1 + ((x - b)/\gamma)^2)$. Bins with less than 20 cells or R^2 of fit lower than 0.8 were omitted. Linear regressions of the baseline FRs vs. the function's peak and FWHM were calculated to identify correlations between the parameters.

Statistical analyses

Analyses were conducted using GraphPad Prism (version 10.1.2). FRs and myelin signals were fit with repeated measure ANOVAs or mixed-effect models when there were missing data points. The mixed models used a compound symmetry covariance matrix and were fit using Restricted Maximum Likelihood. In the absence of missing values, this method gives the same *P* values and multiple comparisons tests as a repeated-measures ANOVA. Data fit was confirmed by checking QQ plot. *Post hoc* comparisons used Dunnett's test to compare with baseline and Tukey's HSD for additional comparisons. Pearson's correlation was used to evaluate relationships between different variables. A Mann-Kendall test was used to detect monotonic trends. A significance threshold of $P < 0.05$ was used for all statistical tests. Details on statistical effect sizes may be found in the Supplementary Statistical Data.

Data availability

Data related to this study will be available from the corresponding author upon reasonable request.

Acknowledgements

The authors would like to thank Drs. Christopher Nelson and Xuefeng (Chris) Liu for helpful comments and suggestions, Mr. Anthony Chomyk for help with tissue histology, as well as to Drs. Monica Boyle, Kevin Dines, and Mrs. Iliana Ruiz for input on the study design.

Author contributions

H.D. and B.T. conceived the project. H.D. and A.D. designed the study and interpreted the results. A.D. performed all surgeries. A.D., J.B. and J.I. performed recording experiments. A.D., H.T., J.B., S.B., J.I., G.T., P.A., S.S., J.M., and P.I. contributed to the data analysis. A.D., and H.D., wrote the manuscript with comments from all authors.

Funding

This study was supported by Bristol-Myers Squibb. The funder had no role in the data collection or analysis, decision to publish, or preparation of the manuscript.

Competing interests

The authors declare no competing interests.

Supplementary material

Supplementary material is available online.

References

1. Stadelmann C, Timmler S, Barrantes-Freer A, Simons M. Myelin in the central nervous system: structure, function, and pathology. *Physiological reviews*, (2019).

2. Geurts JJ, *et al.* Extensive hippocampal demyelination in multiple sclerosis. *Journal of Neuropathology & Experimental Neurology* **66**, 819-827 (2007).

3. Huang WJ, Chen WW, Zhang X. Multiple sclerosis: Pathology, diagnosis and treatments. *Experimental and therapeutic medicine* **13**, 3163-3166 (2017).

4. Dutta R, *et al.* Demyelination causes synaptic alterations in hippocampi from multiple sclerosis patients. *Annals of neurology* **69**, 445-454 (2011).

5. Lucchinetti C, Brück W, Parisi J, Scheithauer B, Rodriguez M, Lassmann H. Heterogeneity of multiple sclerosis lesions: implications for the pathogenesis of demyelination. *Annals of Neurology: Official Journal of the American Neurological Association and the Child Neurology Society* **47**, 707-717 (2000).

6. Bierhansl L, Hartung H-P, Aktas O, Ruck T, Roden M, Meuth SG. Thinking outside the box: non-canonical targets in multiple sclerosis. *Nature reviews Drug discovery* **21**, 578-600 (2022).

7. Denic A, Johnson AJ, Bieber AJ, Warrington AE, Rodriguez M, Pirko I. The relevance of animal models in multiple sclerosis research. *Pathophysiology* **18**, 21-29 (2011).

8. Vega-Riquer JM, Mendez-Victoriano G, Morales-Luckie RA, Gonzalez-Perez O. Five decades of cuprizone, an updated model to replicate demyelinating diseases. *Current neuropharmacology* **17**, 129-141 (2019).

9. Castillo-Rodriguez MdlA, *et al.* Astroglial and oligodendroglial markers in the cuprizone animal model for de-and remyelination. *Histochemistry and cell biology* **158**, 15-38 (2022).

10. Zirngibl M, Assinck P, Sizov A, Caprariello AV, Plemel JR. Oligodendrocyte death and myelin loss in the cuprizone model: an updated overview of the intrinsic and extrinsic causes of cuprizone demyelination. *Molecular neurodegeneration* **17**, 34 (2022).

11. Baltan S, *et al.* Neuronal hibernation following hippocampal demyelination. *Acta neuropathologica communications* **9**, 1-15 (2021).

12. Das A, *et al*. Reversible loss of hippocampal function in a mouse model of demyelination/remyelination. *Frontiers in cellular neuroscience* **13**, 588 (2020).

13. Della-Flora Nunes G, *et al*. Incomplete remyelination via therapeutically enhanced oligodendrogenesis is sufficient to recover visual cortical function. *Nature Communications* **16**, 732 (2025).

14. Dana H, *et al.* Sensitive red protein calcium indicators for imaging neural activity. *Elife* **5**, e12727 (2016).

15. Dana H, *et al.* Thy1 transgenic mice expressing the red fluorescent calcium indicator jRGECO1a for neuronal population imaging in vivo. *PloS one* **13**, e0205444 (2018).

16. Farrar MJ, Wise FW, Fetcho JR, Schaffer CB. In vivo imaging of myelin in the vertebrate central nervous system using third harmonic generation microscopy. *Biophysical journal* **100**, 1362-1371 (2011).

17. Weigelin B, Bakker G-J, Friedl P. Third harmonic generation microscopy of cells and tissue organization. *Journal of Cell Science* **129**, 245-255 (2016).

18. Green AJ, *et al.* Clemastine fumarate as a remyelinating therapy for multiple sclerosis (ReBUILD): a randomised, controlled, double-blind, crossover trial. *The Lancet* **390**, 2481-2489 (2017).

19. Assessment of Clemastine Fumarate as a Remyelinating Agent in Acute Optic Neuritis (ReCOVER).). ClinicalTrials.gov.

20. Gibson EM, *et al.* Neuronal activity promotes oligodendrogenesis and adaptive myelination in the mammalian brain. *Science* **344**, 1252304 (2014).

21. Kalincik T, *et al.* Sex as a determinant of relapse incidence and progressive course of multiple sclerosis. *Brain* **136**, 3609-3617 (2013).

22. Villoslada P, Steinman L. New targets and therapeutics for neuroprotection, remyelination and repair in multiple sclerosis. *Expert opinion on investigational drugs* **29**, 443-459 (2020).

23. Mei F, *et al.* Accelerated remyelination during inflammatory demyelination prevents axonal loss and improves functional recovery. *Elife* **5**, e18246 (2016).

24. Targeting Residual Activity By Precision, Biomarker-Guided Combination Therapies of Multiple Sclerosis (TRAP-MS).). ClinicalTrials.gov.

25. Percie du Sert N, *et al.* The ARRIVE guidelines 2.0: Updated guidelines for reporting animal research. *Journal of Cerebral Blood Flow & Metabolism* **40**, 1769-1777 (2020).

26. Dombeck DA, Harvey CD, Tian L, Looger LL, Tank DW. Functional imaging of hippocampal place cells at cellular resolution during virtual navigation. *Nature neuroscience* **13**, 1433-1440 (2010).

27. Lee JS, Briguglio JJ, Cohen JD, Romani S, Lee AK. The statistical structure of the hippocampal code for space as a function of time, context, and value. *Cell* **183**, 620-635. e622 (2020).

28. Thevenaz P, Ruttimann UE, Unser M. A pyramid approach to subpixel registration based on intensity. *IEEE transactions on image processing* **7**, 27-41 (1998).

29. Stringer C, Wang T, Michaelos M, Pachitariu M. Cellpose: a generalist algorithm for cellular segmentation. *Nature Methods* **18**, 100-106 (2021).

30. Deneux T, *et al.* Accurate spike estimation from noisy calcium signals for ultrafast three-dimensional imaging of large neuronal populations in vivo. *Nature communications* **7**, 12190 (2016).

31. Sheintuch L, *et al.* Tracking the same neurons across multiple days in Ca2+ imaging data. *Cell reports* **21**, 1102-1115 (2017).